

The Energetic Cost of the Action Potential: Bond Graph Modelling of Electrochemical Energy Transduction in Excitable Membranes

Peter J. Gawthrop^{1,2}, Ivo Siekmann¹, Tatiana Kameneva², Susmita Saha³,
Michael R. Ibbotson^{3,4}, and Edmund J. Crampin^{1,5,6}

¹Systems Biology Laboratory, Melbourne School of Engineering, University of Melbourne, Victoria
3010, Australia

²Department of Electrical and Electronic Engineering, The University of Melbourne, Australia.

³National Vision Research Institute, Australian College of Optometry, Australia.

⁴Centre of Excellence for Integrative Brain Function, Dept. Optometry and Vision Sciences, The
University of Melbourne, Australia.

⁵School of Mathematics and Statistics, University of Melbourne, Victoria 3010, Australia

⁶School of Medicine, University of Melbourne, Victoria 3010, Australia

December 11, 2021

Abstract

The energy consumed during an action potential event must be replaced, ultimately by the metabolic system of the organism. As discussed by a number of authors including (2, 5, 10, 17, 21, 38–40), there is a trade-off between the speed of an action potential event and energy consumption and, moreover, this consumption can be optimised by adjusting ion channel density (17, 20) and gating time constants (17, 38). The energy consumption is dependent on both species and type of neuron (39).

The influx of Na^+ (5, 17) is often taken as a proxy for energy consumption. For example, as discussed by Hasenstaub et al. (17), 3Na^+ ions can be expelled using 1 ATP molecule within the sodium-potassium pump (Na^+ , K^+ , ATPase). Thus $1/3$ of the Na^+ can be taken as a proxy for energy consumption. In contrast, this paper presents an energy based model of action potentials and thus can be directly used to compute energy consumption in both healthy and diseased neurons.

These results are illustrated by comparing the energy consumption of healthy and degenerative retinal ganglion cells using both simulated and *in vitro* data.

December 11, 2021

Contents

| | | |
|----------|---|-----------|
| 1 | INTRODUCTION | 3 |
| 2 | MODELLING APPROACH | 5 |
| 2.1 | Bond Graph Models of Biochemical Reactions | 6 |
| 2.2 | Power and Energy | 7 |
| 2.3 | Modelling Electrochemical Transduction using Bond Graphs | 7 |
| 2.4 | Bond Graph modelling of ionic current flow | 11 |
| 2.5 | Bond Graph Modelling of Voltage Gating | 15 |
| 2.6 | Energy Flow in the Hodgkin Huxley Action Potential | 20 |
| 2.7 | Energy consumption in healthy and degenerative retinal ganglion cells | 24 |
| 3 | DISCUSSION | 24 |
| 4 | ACKNOWLEDGEMENTS | 26 |
| 5 | AUTHOR CONTRIBUTIONS | 26 |
| 6 | DATA ACCESSIBILITY | 26 |
| A | SUPPORTING MATERIAL | 32 |
| A.1 | Example: Application of the proposed methodology to calculate the energy consumption in healthy and degenerative retinal ganglion cells | 32 |
| A.1.1 | Methods | 32 |

1 INTRODUCTION

Understanding the biophysical processes which underlie the generation of the action potential in excitable cells is of considerable interest, and has been the subject of intensive mathematical and computational modelling. Since the early work of Hodgkin and Huxley (19) on modelling the ionic mechanisms which give rise to the action potential in neurons, mathematical models of the action potential have incorporated ever-increasing biophysical and ionic detail (18), and have been formulated to describe both normal and pathophysiological mechanisms.

Generation of the action potential comes at a metabolic cost. Energy is required to maintain the imbalance of ionic species across the membrane, such that when ion channels open there is a flux of ions (current) across the membrane – initially carried by sodium ions – generating rapid membrane depolarisation (the upstroke of the action potential). Each action potential reduces the ionic imbalance and each ionic species needs to be transported across the membrane against an adverse voltage gradient to restore the imbalance – this requires energy.

The role of energy in neural systems has been widely discussed in the literature (5, 10, 17, 38–40) and it has been suggested that metabolic cost is a unifying principle underlying the functional organisation and biophysical properties of neurons (17, 34). Furthermore, Beal (3) posed the question “Does impairment of energy metabolism result in excitotoxic neuronal death in neurodegenerative illnesses?” More recently, it has been suggested (9, 52, 53) that an energy-based approach is required to elucidate neuro-degenerative diseases such as Parkinson’s disease.

In such studies, the flow of Na^+ across the membrane is taken as a proxy for energy consumption associated with action potential generation, as Na^+ has to be pumped back across the membrane by an energy-consuming ATPase reaction. This energetic cost is often quoted as an equivalent number of ATP molecules required to restore the ionic concentration gradient through activity of the sodium-potassium ATPase (the Na pump), as calculated via stoichiometric arguments. While this provides a useful indication of energetic cost, this is however an imprecise approach, which cannot produce reliable estimates of energy flows under all conditions (physiological and pathophysiological). What is required instead is a way of simulating and calculating the actual energy flows associated with these ionic movements through a physically-based modelling approach.

Techniques for modelling dynamic systems, including biological systems, lie on a spectrum with mechanistic physically-based modelling at one end and empirical data-driven modelling at the other. The former has the advantage of being based on physical principles and therefore obeying key conservation laws but may be complex and difficult to match up with measured data. On the other hand the latter is potentially simpler and can be designed for fitting to data but there is no guarantee that it will obey conservation laws and will not provide any physical insight. This tension between physical and empirical modelling can be removed by introducing the concept of *physically-plausible models*.

Physically-plausible models are models which, although they do not pretend to be an accurate models of a particular physical system, are themselves models of physical systems, share key physical properties and behaviours of the actual system, and have parameters which relate to physical constants (12). Typically, the physically-plausible model will be simpler than the system itself. The advantages of having a simpler model are that it is easier to understand a simple model

than a complex model, and the computational and numerical aspects are simpler. The advantages of a physical model are that the parameters of a physical model have a clearer interpretation than those of a purely empirical model, and the behaviour of the model can be understood in physical terms. Such physically-plausible models may be represented by a bond graph, described below.

In the context of excitable membranes the FitzHugh–Nagumo model (27, § 5.2), (28, Chapter 7) is an example of an empirical model of the action potential.¹ Although originally developed to provide a mathematically tractable model of excitability; the FitzHugh–Nagumo equations have been used to illustrate non-linear state and parameter estimation from noisy data by Voss et al. (50) and discussed in the context of neural control engineering by Schiff (37, Chapter 5). On the other hand, the model of Hodgkin and Huxley (19), as discussed by Keener and Sneyd (27, § 5.1) & Koch (28, Ch 6), is an example of a physically-plausible model: a physical system, an equivalent electrical circuit, is used to model the squid giant axon; however, the gating equations used by Hodgkin and Huxley (19) are empirical.

Hodgkin and Huxley (19) use an electrical circuit as an *analogy* of a electrochemical system; as discussed by Maxwell (31), this enables insights and methods from one domain (electrical) to be applied in another (electrochemical). Moreover, collapsing the two domains of chemistry and electricity into a single domain makes the system easier to comprehend and analyse and it has been the mainstay of neurocomputation for over 60 years (6). This generalised use of analogies in modelling dynamical systems is well established in the fields of physics and engineering (30, 41) and is based on the unifying principle of energy conservation and modelling the transduction of energy between different physical domains. With the few exceptions noted below, such approaches have not been systematically applied in the life sciences. In this paper, the use of analogies to model systems involving electrochemical transduction is explored using the the Bond Graph approach.

The Bond Graph is an energy-based modelling approach which provides a systematic framework for physically-plausible models. A comprehensive account of the use of Bond Graphs to model physical systems is given in the textbooks of Gawthrop and Smith (11), Mukherjee et al. (32), Borutzky (4) and Karnopp et al. (25) and a tutorial introduction for control engineers is given by Gawthrop and Bevan (13). The Bond Graph approach has previously been applied to biochemical reaction networks by Oster et al. (35, 36) and to chemical reactions by Cellier (7) and Greifeneder and Cellier (16).

Gawthrop and Crampin (14) build on the work of Oster et al. (35, 36) to show how the bond graph approach can be used to model common biochemical cycles such as phosphorylation/dephosphorylation so that the resultant model is thermodynamically compliant and the structural properties of the bond graph are related to the stoichiometric matrix, conserved moieties and flux paths. Gawthrop et al. (15) extend this method to consider hierarchical bond graph modelling of biochemical networks such as glycogenolysis. In particular, a hierarchical energy-based formulation of the Hodgkin and Huxley (19) membrane model is developed with simple species and reaction components at the base layer and ion channel and gating models at intermediate layers to give the final energy-based model, represented as a Bond Graph. This model is then used to quantify the energy flow associated with generation of the action potential.

¹Other empirical models include those of Morris–Lecar and Pinsky–Rinzel (44, Chapter 8).

This theoretical approach is then applied to analyse energy consumption in retinal ganglion cells based on *in vitro* experimental data collected and analysed from retinal ganglion cells (RGCs) of wild-type (WT) and degenerative (RD1) mice. Our use of the RD1 degenerate retina mouse model ensures that the outcomes of this project are directly relevant to human patients since RD1 mice have a degenerate retina that has distinct similarities to that observed in human patients with *retinitis pigmentosa* – a set of hereditary retinal diseases that results from the degenerative loss of the photoreceptors in the retina.

A virtual reference environment (22) is available for this paper at https://github.com/uomsystemsbiology/energetic_cost_reference_environment.

2 MODELLING APPROACH

Bond graphs are a graphical way to represent the flow of energy through a system. The bond graph method provides a set of rules by which systems may be described, such that underlying physical conservation principles are adhered to. The bond graph itself represents the equations underlying the graph; which can be constructed, manipulated and analysed through the structure and properties of the bond graph.

A bond graph consists of ‘signal quantities’, generalised as ‘effort’ and ‘flow’, which are manipulated by ‘components’ and coupled together using ‘connectors’. The quantities effort and flow are chosen such that the product of effort and flow is power. Examples of effort include Force, Voltage and Pressure. Corresponding examples of flow are Velocity, Current and fluid Flow Rate. The products of each of these pairs of effort and flow is power. Components in the bond graph include sources of effort or flow (**SS**), capacitors or springs which store energy (**C**), resistors or dampers which dissipate energy (**R**), and transducers (or transformers) (**TF**) which transmit and convert, but do not dissipate, power². Power bonds (or more simply ‘bonds’, drawn as harpoons, \rightarrow connect components, such that components which are connected share the same effort and flow. Bonds can be optionally annotated with specific effort and flow variables, for example $\frac{e}{f}$. ‘Junctions’ allow parallel (**0** junction) and series (**1** junction) connections to be made. The efforts on bonds impinging on an **0** junction are equal, and flows sum to zero (equivalent to Kirchhoff’s first law for electric circuits, where effort is equivalent to voltage and flow is equivalent to current); while efforts sum to zero and flows are equal for a **1** junction (equivalent to Kirchhoff’s second law).

Once a system is represented in this manner, the bond graph ensures that properties such as energy and mass are conserved (in the sense that any dissipative processes are directly accounted for, and any inputs to or losses from the system are quantified). The bond graph can be used to generate the governing system of equations (dynamical system) for simulation, however there are a wide range of other possibilities, including computational tools for construction and manipulation. For further details are given in the textbooks(4, 11, 25, 32, 51). Of particular

²Because a given type of component usually occurs more than once in a given system, the ‘colon’ notation is adopted to distinguish between different instances of each component type: the symbol preceding the colon identifies the type of component, and the label following the colon identifies the particular instance

relevance to modelling of cellular systems, the bond graph method allows formal simplification and approximation (13), and also allows hierarchical modelling and representation of complex systems Cellier (8), Gawthrop et al. (15). The following sections provide a brief introduction to the material used in this paper.

2.1 Bond Graph Models of Biochemical Reactions

It is assumed that in the body biochemical reactions occur under conditions of constant pressure (isobaric) and constant temperature (isothermal). Under these conditions, the chemical potential μ_A of substance A is given (1) in terms of its mole fraction χ_A as:

$$\mu_A = \mu_A^* + RT \ln \chi_A \text{ J mol}^{-1} \quad (1)$$

where μ_A^* is the value of μ_A when A is pure ($\chi_A = 1$), $R = 8.314 \text{ JK}^{-1} \text{ mol}^{-1}$ is the universal gas constant, T is the absolute temperature and \ln is the natural (or Napierian) logarithm.

The key to modelling chemical reactions by bond graphs is to determine the appropriate effort and flow variables. As discussed by Oster et al. (35, 36), the appropriate *effort* variable is *chemical potential* μ and the appropriate *flow* variable is molar flow rate v .

In the context of chemical reactions, the bond graph **C** component of is defined by Equation (1) as:

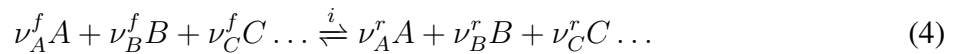
$$\dot{x}_A = v_A \text{ mol sec}^{-1} \quad \mu_A = RT \ln K_A x_A \text{ J mol}^{-1} \quad (2)$$

where x_A is the molar amount of A and the *thermodynamic constant* K_A is given by

$$K_A = \frac{1}{n_{total}} \exp \frac{\mu_A^*}{RT} \quad (3)$$

where n_{total} is the total number of moles in the mixture.

We follow Oster et al. (36) in describing chemical reactions in terms of the *Marcelin – de Donder* formulae as discussed by Van Rysselberghe (49) and Gawthrop and Crampin (14). In particular, given the i th reaction (36, (5.9)):



where the stoichiometric coefficients ν are either zero or positive integers and the *forward affinity* A_i^f and the *reverse affinity* A_i^r are defined as:

$$A_i^f = \nu_A^f \mu_A + \nu_B^f \mu_B + \nu_C^f \mu_C \dots \quad (5)$$

$$A_i^r = \nu_A^r \mu_A + \nu_B^r \mu_B + \nu_C^r \mu_C \dots \quad (6)$$

The i th reaction flow v_i is then given by:

$$v_i = \kappa_i (v_0^+ - v_0^-) \quad (7)$$

$$\text{where } v_0^+ = e^{\frac{A_i^f}{RT}} \text{ and } v_0^- = e^{\frac{A_i^r}{RT}} \quad (8)$$

Note that the arguments of the exponential terms are dimensionless as are v_0^+ and v_0^- . The units of the reaction rate constant κ_i are those of molar flow rate: mol sec⁻¹.

The i th reaction flow v_i depends on the forward and reverse affinities A_i^f and A_i^r but cannot be written as the difference between the affinities; hence, unlike the electrical **R** component, it cannot be written as a one port component with the flow dependent on the difference between the efforts. However, as discussed by Gawthrop and Crampin (14), a two port resistive component, the **Re** component, can be used to model the reaction flow (7). As discussed below, the bond graph **TF** component provides a mechanism for connecting different physical domains. This paper shows that it can be used to connect the chemical (chemical potential and molar flow) and electrical (voltage and current) domains to give a thermodynamically consistent integrated model.

2.2 Power and Energy

As noted above, the rate of energy transfer, or power flow, of a bond associated with substance A is $p_A = \mu_A v_A$ W where μ_A is the chemical potential defined in Equation (1) and v_A is the molar flow rate. This section looks at two particular cases relevant to the methods of this paper.

In the particular case that substance A occurs on each side of a membrane and is replaced on one side, and removed at the other, at a variable rate v_A so that it remains at a fixed concentration on each side, the the net external power associated with substance A is:

$$p_{eA} = (\mu_i - \mu_r) v_A \quad (9)$$

where μ_i and μ_r are the internal and external chemical potentials respectively. Using Equation (1)

$$\begin{aligned} \mu_i - \mu_r &= RT (\ln \chi_i - \ln \chi_r) = RT \ln \frac{\chi_i}{\chi_r} \\ &= RT \ln \frac{c_i}{c_r} = G_A \end{aligned} \quad (10)$$

where c_i and c_r are the internal and external concentrations of substance A ; G_A can be interpreted as the Gibbs free energy change of moving A from inside to outside in this particular case.

In the case of the i th chemical reaction component, the energy flow in is the product of the reaction flow v_i and the forward affinity A_i^f of Equation (5) and the energy flow out is the product of the reaction flow v_i and the reverse affinity A_i^r of Equation (6). Thus the power dissipated in the i th chemical reaction is:

$$p_i = A_i^f v_i - A_i^r v_i = A_i v_i \quad (11)$$

where the reaction affinity A_i is given by $A_i = A_i^f - A_i^r$.

2.3 Modelling Electrochemical Transduction using Bond Graphs

As an energy-based method, the bond graph representation is particularly appropriate for modelling systems with multiple energy domains – in this case chemical and electrical. In order

to use the bond graph method to provide a physically-plausible model for the electrochemical properties of the cell membrane, it is necessary to extend the analysis above to incorporate electrical energy transduction, as required for movement of charged ions across the trans-membrane electric potential.

We consider a membrane which separates two solutions with different ionic concentrations and different electrical potentials V_i and V_e respectively, such that the voltage difference V across the membrane (the membrane potential) is given by:

$$V = V_i - V_e \quad (12)$$

For each ionic species, the membrane ionic flow rate v_{ion} mol sec⁻¹ is modulated by the voltage V V and the voltage V is modulated by the ionic flow rate. Because the ions carry charge, passage across the membrane involves two forms of energy: chemical, in respect of any concentration gradient across the membrane; and electrical, in respect of the movement of charge across an electrical potential (membrane potential). Analogously to chemical energy flow, described above, electrical energy flow is modelled as the product of two variables: voltage V and current i . As discussed in the bond graph context by Karnopp (24), the two energy domains are coupled by noting that the molar flow of ions through the membrane v_{ion} mol sec⁻¹ is related to the current flow i A by:

$$i = zFv_{ion} \quad (13)$$

where z is the (integer) ionic charge and F Faraday's constant which has the approximate value $F \approx 96.5 \times 10^3 \text{C mol}^{-1}$. Thus, for example, an ion with unit charge and flow rate of 1 nmol sec⁻¹ is equivalent to a current of about $96.5 \mu\text{A}$. The bond graph representation for electrochemical transduction is shown in Figure 1. With reference to Figure 1(a), equation (13) is modelled by the bond graph transformer component **TF:zF** where μ_V is introduced as the *chemoelectrical potential*: the chemical potential corresponding to the membrane voltage V . As discussed by Karnopp et al. (25) and Gawthrop and Crampin (14), **TF** components transmit, but do not dissipate power, so $\mu_V v_{ion} = Vi$ and thus the flow equation (13) also implies that the chemoelectrical potential μ_V is given by

$$\mu_V = zFV \quad (14)$$

Thus, for example, a voltage of 1mV is equivalent to a chemical potential of an ion with unit charge of about 96.5J mol^{-1}

Stoichiometric analysis of biochemical reactions has a bond graph interpretation in terms of the bond graph structure. As a structural matrix, the stoichiometric matrix for biochemical systems contains integer entries corresponding to reaction stoichiometry. The bond graph describing electrochemical transduction in Figure 1(a) contains transformers connecting the electrical and chemical domains and the electrochemical transformer contains the Faraday constant F which is not an integer. For this reason, it is useful as shown in Figure 1(b) to split the component **TF:zF** into two **TF** components in series: **TF:z** and **TF:F**. Thus **TF:z** corresponds to the integer, but ion-dependent charge, z , and **TF:F** to the universal constant, but non-integer, F . **TF:z** will be referred to as the *electrostoichiometric transformer*.

Furthermore, the electrical component **C:Q** and the electrochemical transformer **TF:F** component may be replaced by a single *electrogenic capacitor* **C:x_m** as in Figure 1(c). Assuming

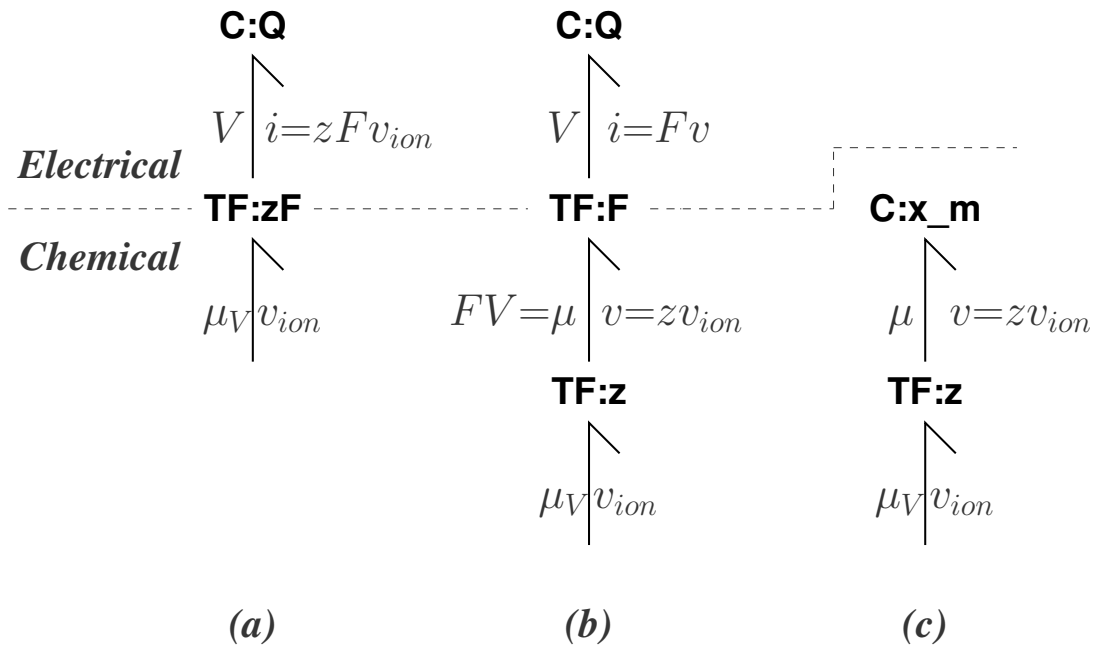


Figure 1: Electrochemical Transduction. (a) The transduction of ion membrane flow v_{ion} into electrical current i is represented by $\mathbf{TF:zF}$ where where z is the ionic charge and F Faraday's constant; $\mathbf{C:Q}$ represents the membrane capacitance containing electrical charge Q and μ_V is the *chemoelectrical potential*: the chemical potential corresponding to the membrane voltage V (b) $\mathbf{TF:zF}$ is split into two series components $\mathbf{TF:z}$ & $\mathbf{TF:F}$. (c) The electrical capacitor $\mathbf{C:Q}$ and the electrochemical transducer $\mathbf{TF:F}$ are combined into chemo-equivalent capacitor $\mathbf{C:x_m}$ containing x_m moles of charge. $\mathbf{C:x_m}$ is analogous to a chemical species, and $\mathbf{TF:z}$ to a stoichiometric transformer.

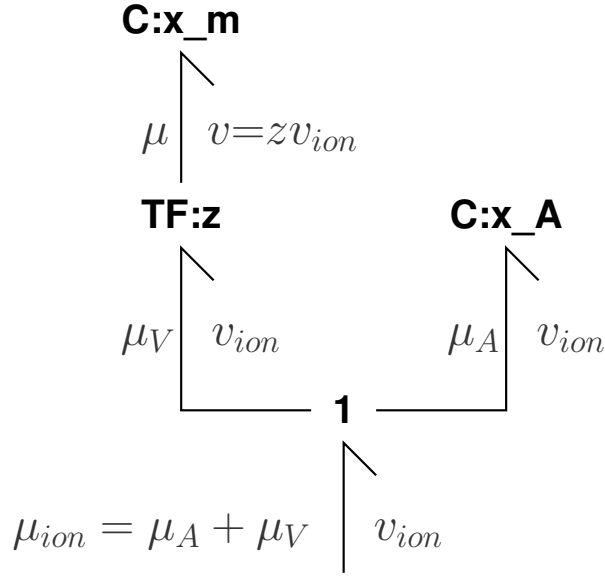


Figure 2: Combined chemoelectrical and chemical potentials

that the electrical capacitor has the constant capacitance C (CV^{-1}), and with reference to Figure 1(b)

$$\mu = FV \quad V = \frac{Q}{C} \quad \dot{Q} = I \quad I = Fv \quad (15)$$

While the electrogenic capacitor $\mathbf{C}:\mathbf{x}_m$ is linear and therefore cannot be written in the logarithmic form of Equation (2), it is convenient to write the defining equations in a similar form: with reference to Figure 1(c)

$$\mu_V = RTK_e x_m \quad \dot{x}_m = v \quad (16)$$

Comparing Equations (15) and (16), it follows that:

$$K_e = \frac{F^2}{CRT} = \frac{V_e}{V_N} \text{mol}^{-1} \quad (17)$$

where $V_e = \frac{F}{C} \text{Vmol}^{-1}$ and $V_N = \frac{RT}{F} \text{V}$

V_e is the *equivalent voltage* associated with each mole of charge and is dependent on the electrical capacitance C . V_N is related to the *Nernst potential* and is temperature dependent.

In summary, $\mathbf{C}:\mathbf{x}_m$ is analogous to a chemical species (but with a non-logarithmic characteristic), and $\mathbf{TF}:z$ is analogous to the stoichiometric transformers discussed by Oster et al. (35, 36), Greifeneder and Cellier (16) and Gawthrop and Crampin (14).

Figure 2 corresponds to a single ionic species A , with integer charge z , flowing across a membrane at a rate v_{ion} . The electrogenic capacitor $\mathbf{C}:\mathbf{x}_m$ and the electrostoichiometric transformer

TF: z represent the voltage-related energy and the chemical capacitance **C**:**A** the chemical potential. The **1** junction ensures that the flow v_{ion} corresponds to both electrical and chemical flow and implies that the net chemical potential μ_{ion} is the sum of the chemical potential μ_A and the chemoelectrical membrane potential $\mu_V = zFV$. This is the standard electrostatic contribution to the electrochemical potential:

$$\mu_{ion} = \mu_A + \mu_V = \mu_A + zFV \quad (18)$$

In general, as discussed below, the electrogenic capacitor will correspond to the net flow of more than one charged species.

2.4 Bond Graph modelling of ionic current flow

With these developments, we now revisit the Hodgkin and Huxley (19) model. Hodgkin and Huxley (19) model an ion channel as a linear conductance g_{ion} , modulated by a function G_{ion} in series with the Nernst potential represented by a voltage source V_{ion} (see Figure 3).

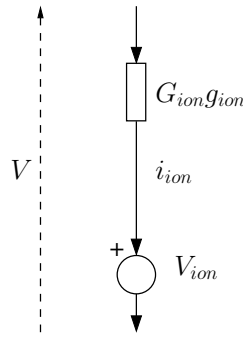


Figure 3: The Hodgkin-Huxley Axon Model

In Hodgkin and Huxley's original study, there are two ionic species considered: sodium Na^+ and potassium K^+ and a corresponding ion channel for each. The conductance is modulated by the membrane potential V and the voltage source V_{ion} is a function of the internal and external ion concentrations. Thus for each ion, the current i is:

$$i_{ion} = g_{ion} G_{ion}(V, t)(V - V_{ion}) \quad (19)$$

where $0 \leq G_{ion}(V, t) \leq 1$ is the gating function, which is a dynamic function of membrane potential V . Voltage gating will be considered below.

It is convenient to normalise equation (19) by defining

$$\bar{V} = \frac{V}{V_N} \quad (20)$$

$$\bar{V}_{ion} = \frac{V_{ion}}{V_N} \quad (21)$$

$$\tilde{V}_{ion} = \frac{V - V_{ion}}{V_N} = \bar{V} - \bar{V}_{ion} \quad (22)$$

where V_N given by (17) and rewriting Equation (19) as:

$$\dot{i}_{ion} = g_{ion} G_{ion}(V, t) V_N \tilde{V}_{ion} \quad (23)$$

In terms of ionic flow v_{ion} , Equation (23) becomes:

$$\begin{aligned} v_{ion} &= \frac{1}{F} \dot{i}_{ion} = \frac{g_{ion} G_{ion}(V, t) V_N \tilde{V}_{ion}}{F} \\ &= \kappa_{HH} c_e G_{ion}(V, t) \tilde{V}_{ion} \end{aligned} \quad (24)$$

$$\text{where } \kappa_{HH} = \frac{g_{ion} V_N}{F c_e} \quad (25)$$

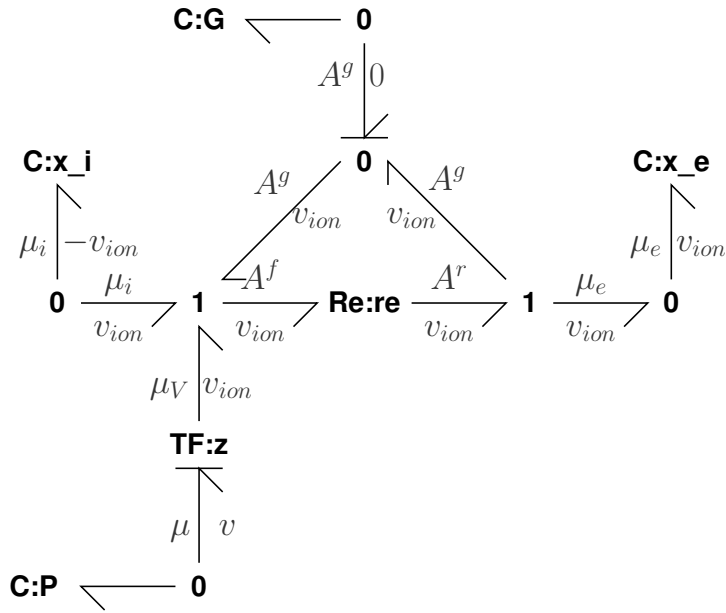


Figure 4: Ion-channel Model: Reaction analogy. With reference to reaction (26), the ion X_e external to the membrane is represented by $\mathbf{C}:x_e$, the ion X_i internal to the membrane is represented by $\mathbf{C}:x_i$ and the internal to external molar flow rate is v_{ion} . $\mathbf{TF}:z$ is electrostoichiometric transformer where z is the integer ionic charge. $\mathbf{C}:P$ represents the membrane potential as an electrogenic capacitance with electrogenic potential μ and electrogenic flow v . The ionic flow is determined by the reaction component $\mathbf{Re}:re$ and modulated by the gating affinity A^g associated with the $\mathbf{C}:G$. The two components $\mathbf{C}:G$ and $\mathbf{C}:P$ and associated junctions may be related by ports; this enables the model to be reused within a hierarchical framework.

In order to produce a physically plausible model for the flow of ions through the open pore of an ion channel, a choice must be made about the appropriate physical analogy and corresponding mathematical formulation. In Figure 1, the electrical domain is given a chemical analogy in terms of the electrostoichiometric transformer $\mathbf{TF}:z$ and the electrogenic capacitor $\mathbf{C}:x_m$; this analogy is pursued here by representing a membrane ion channel by a chemical reaction:



where X_i is the internal ion species, X_e the external ion species, P the electrogenic species representing the membrane potential and G the *gating species* to be examined below. G is analogous to an *enzyme*. In a similar manner to that presented by Gawthrop and Crampin (14, Figure 1), Equation (26) is represented in bond graph form in Figure 4. The flow into $\mathbf{C}:x_i$ and $\mathbf{C}:x_e$ is $-v_{ion}$ and v_{ion} respectively and the corresponding chemical potentials are (14):

$$\mu_i = RT \ln K_i x_i \quad (27)$$

$$\mu_e = RT \ln K_e x_e \quad (28)$$

$$\text{where } K_i = \frac{K_{ion}}{C_i} \quad (29)$$

$$\text{and } K_e = \frac{K_{ion}}{C_e} \quad (30)$$

$$\text{where } K_{ion} = \exp \frac{\mu^0}{RT} \quad (31)$$

μ^0 is the standard chemical potential for the ion and the volumetric capacities of the interior and exterior are C_i and C_e respectively.

The reaction flow v_{ion} is modelled by the **Re:re** component in Figure 4 as part of the chemical analogy of a voltage-gated ion channel and is given by Equation (7). As noted above, membrane flow rate v_{ion} is modulated by the voltage V ; in addition it is gated by the voltage V (in voltage-gated channels) and by a ligand (in ligand-gated channels). In this paper, such modulation is regarded as analogous to the effect of an enzyme in an enzyme-catalysed reaction. In particular the *gating affinity* A^g is added to both sides of the reaction as in Figure 4 in the same way as in Gawthrop and Crampin (14, Figure 2e). The second port **SS:[g]** imposes the gating affinity A^g and the corresponding flow $v_g = v_{ion} - v_{ion} = 0$.

The gating affinity A^g is dependent on two characteristics: the characteristics of the model of the ion-channel pore G_{pore} (alternative versions of G_{pore} are described below) and the characteristics of ion-dependent gating G_{ion} . In particular A^g is written as:

$$A^g = \ln G_{pore}(V) + \ln G_{ion}(V) \quad (32)$$

$$\text{or } \exp A^g = G_{pore}(V)G_{ion}(V) \quad (33)$$

From the bond graph of Figure 4 and Equation (14), it follows that:

$$\begin{aligned} A^f &= A^g(V) + \mu_i + \mu_V \\ &= A^g(V) + \mu_i + zFV \end{aligned} \quad (34)$$

$$A^r = A^g(V) + \mu_e \quad (35)$$

Using Equations (27) and (7), the corresponding ionic flow is:

$$v_{ion} = \kappa K_{ion} \exp A^g(\bar{V}) (c_i \exp \bar{V} - c_e) \quad (36)$$

$$\text{where } c_i = \frac{x_i}{C_i}, \quad c_e = \frac{x_e}{C_e} \quad (37)$$

and \bar{V} is given by Equation (20). Define \bar{V}_{ion} as the voltage for which v of Equation (36) is zero:

$$c_i \exp \bar{V}_{ion} - c_e = 0 \quad (38)$$

$$\text{hence } \bar{V}_{ion} = \ln \frac{c_e}{c_i} = - \ln \frac{c_i}{c_e} \quad (39)$$

Using Equations (39) and (33), Equation (36) becomes:

$$v_{ion} = \kappa K_{ion} c_e G_{ion}(V) G_{pore}(V) \left(\exp \tilde{V}_{ion} - 1 \right) \quad (40)$$

where \tilde{V}_{ion} is given by (22). $\exp(-\tilde{V}_{ion})$ is known as the *Ussing Flux Ratio* (27, §3.2). This is the ionic flow (ion current) model which will be used in the sequel to construct a Bond Graph model from the Hodgkin Huxley model.

We must now determine an appropriate form for the model of the ion-channel pore, G_{pore} . A key feature of the ionic flow equation (24) for the Hodgkin-Huxley model is that the flow v_{ion} is zero when $\tilde{V}_{ion} = 0$. This feature is shared with the mass action model. In particular, setting $\tilde{V}_{ion} = 0$ in Equation (40) gives $(\exp \tilde{V} - 1) = (1 - 1) = 0$ and thus $v_{ion} = 0$. This fact makes it possible to choose the model-dependent function $G_{pore}(V)$ so that Equation (40) is identical to the Hodgkin-Huxley model of Equation (24). In particular:

$$G_{pore} = G_{HH}(V) = \begin{cases} 1 & \tilde{V} = 0 \\ \frac{\tilde{V}_{ion}}{\exp \tilde{V}_{ion} - 1} & \tilde{V}_{ion} \neq 0 \end{cases} \quad (41)$$

Clearly, equation (41) only makes sense if G_{HH} is positive for all \tilde{V} . If $\tilde{V} < 0$, both \tilde{V} and $\exp \tilde{V} - 1$ are negative; if $\tilde{V} > 0$, both \tilde{V} and $\exp \tilde{V} - 1$ are positive; and, as $G_{HH}(0) = 1$, $G_{HH}(\tilde{V})$ is positive for for all \tilde{V} .

A number of alternative physically-based models for the ion channel are available. In particular, the Goldman-Hodgkin-Katz (GHK) model (see Keener and Sneyd (27, § 2.6.3 (2.123)), Koch (28, § 9.1.1)) & Sterratt et al. (44) can be rewritten in a similar form to (40) as:

$$v = \kappa K_0 c_e \bar{V} \frac{\exp \tilde{V} - 1}{\exp \bar{V} - 1} \quad (42)$$

Comparing Equations (40) and (42), it follows that the mass action model (40) and GHK model are the same if the model-dependent function $G_{pore}(V)$ is:

$$G_{pore} = G_{GHK}(V) = \begin{cases} 1 & \bar{V} = 1 \\ \frac{\bar{V}}{\exp \bar{V} - 1} & \bar{V} \neq 1 \end{cases} \quad (43)$$

Note that $G_{GHK}(V)$ (43) is of the same form as $G_{HH}(V)$ (41) except that \tilde{V} is replaced by \bar{V} .

From equations (24) and (40), both the HH and GHK ion channel models give zero ionic flow when the membrane voltage equals the Nernst voltage: that is the models match at $\tilde{V}_{ion} = 0$. Moreover, the GHK model of Equation (42) has a parameter κ that can be chosen to fit the data. In this case, κ is chosen so that the GHK and HH models also match at another voltage; in this case chosen as minus the Nernst voltage. Figure 5 shows the ionic currents plotted against membrane voltage for each of the three channels and they match at the two voltages. The GHK model is used in the sequel.

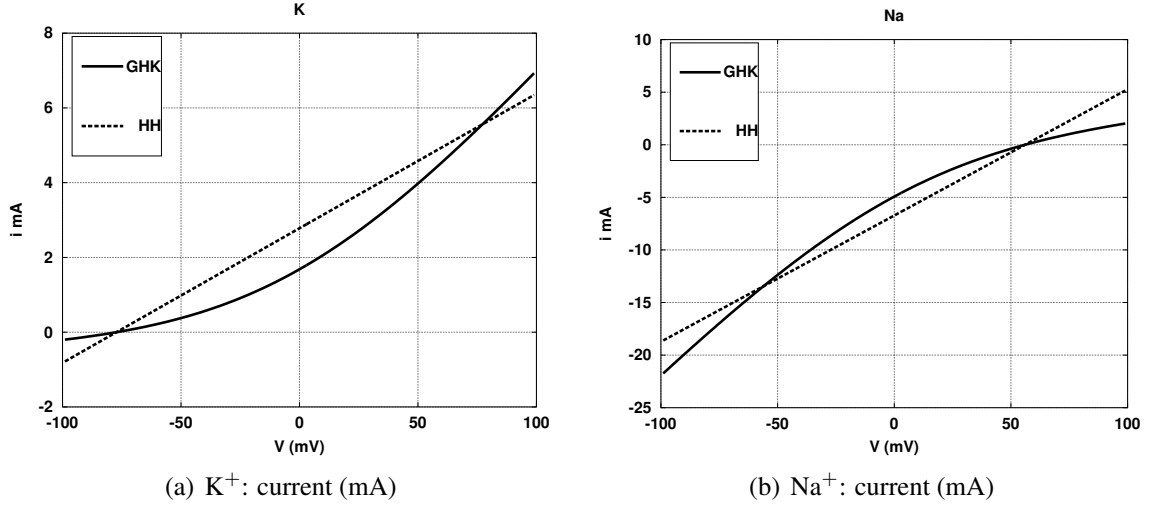


Figure 5: Comparison of current(mA)–voltage(mV) relationships for Na⁺ and K⁺ currents for $G_{pore} = G_{HH}$ and $G_{pore} = G_{GHK}$ models.

| Ion | K ⁺ | Na ⁺ | Leakage |
|--------------------------------|----------------|-----------------|-----------|
| $\kappa \text{ nmol sec}^{-1}$ | 0.046262 | 0.13204 | 0.0014329 |

Table 1: GHK parameter $\kappa \text{ nmol sec}^{-1}$

2.5 Bond Graph Modelling of Voltage Gating

We next turn to the gating function $G_{ion}(V, t)$. Voltage-gating is incorporated into the bond graph model with the voltage-dependent affinity term G_{ion} in Equation (32). Figure 6 shows the three ionic currents from the Hodgkin Huxley model for the two ionic species Na⁺ and K⁺ and the leak current. In each case, they encapsulate the channel model of Figure 4 and the GHK affinity function of Equation (43); they differ in the ion-dependent gating function.

As Hodgkin and Huxley (19) showed, and has been verified many times since (18), the gate function is a dynamical function of voltage. The standard approach is to approximate this dynamical function by a linear first order ODE with voltage dependent coefficients of the form:

$$\frac{dg}{dt} = \alpha(V)(1 - g) - \beta(V)g \quad (44)$$

This can be rewritten in a more convenient form as:

$$\frac{dg}{dt} = -\tau(V)(g_{ss}(V) - g) \quad (45)$$

$$\text{where } \tau(V) = \frac{1}{\alpha(V) + \beta(V)} \quad (46)$$

$$\text{and } g_{ss}(V) = \frac{\alpha(V)}{\alpha(V) + \beta(V)} \quad (47)$$

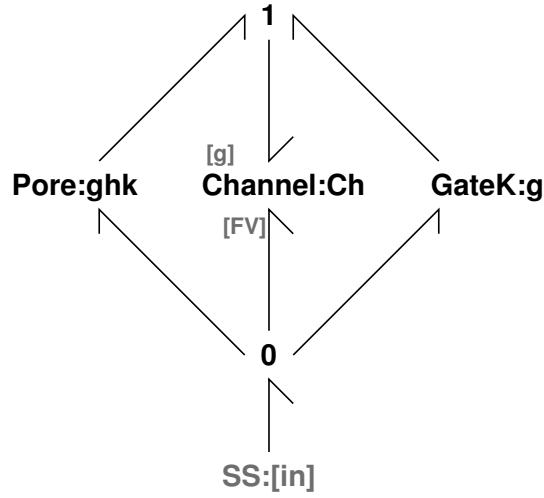


Figure 6: Goldman-Hodgkin-Katz K^+ Channel Model. The Na^+ model is identical except that the right-hand component is replaced by the appropriate gate component. Following the Hodgkin-Huxley model, the leak component is not voltage gated and the right-hand component does not appear. Alternatives to the Goldman-Hodgkin-Katz model are simply obtained by replacing the pore component.

In the particular case that $V = V_0$ is constant, Equation (45) is a linear first order ODE with $g_{ss}(V_0)$ is the steady-state value of g , $\tau(V_0)$ is the corresponding time constant. By the use of multiple gates (with different forms of g_{ss} and τ) per channel is possible to fit quite complicated experimental data (18, 45). In the Hodgkin Huxley model, the gating functions two ionic species Na^+ and K^+ . Following Keener and Sneyd (27, § 5.1.2), the modulating functions G_{ion} can be written as follows. For potassium:

$$G_K = n^4$$

$$\text{where } \frac{dn}{dt} = \alpha_n(1 - n) + \beta_n n \quad (48)$$

and for sodium:

$$G_{Na} = m^3 h$$

$$\text{where } \frac{dm}{dt} = \alpha_m(1 - m) + \beta_m m$$

$$\text{and } \frac{dh}{dt} = \alpha_h(1 - h) + \beta_h h \quad (49)$$

However, this empirical approach does not represent a physically plausible system, as no account is taken of the associated movement of charge or energy dissipated during this process. As discussed by Keener and Sneyd (27, §3.5) and Hille (18, Chapter 2), it is possible to represent ion channel gates as a set of chemical equations incorporating *gating charge* and *gating current*. In

contrast to the empirical approach this has the advantage of making the gates thermodynamically compliant.

In the simplest case consider the voltage-dependent first-order reaction



where there are x_c mol of pseudo substance C and x_o mol of pseudo substance O . The sum of x_c and x_o is a conserved moiety and thus, for each gate, the constant x_g mol can be defined as:

$$x_g = x_c + x_o \quad (51)$$

Thus O represents the fraction of channels $\frac{x_o}{x_g}$ in an open state and C represents the fraction of channels $\frac{x_c}{x_g}$ in a closed state³. Figure 7 (a) shows one possible bond graph representation of such a reaction where the voltage dependence arises in exactly the same way as the channel model of Figure 4.

The molar flow v_g for the gating model shown in Figure 7 (a) is given by

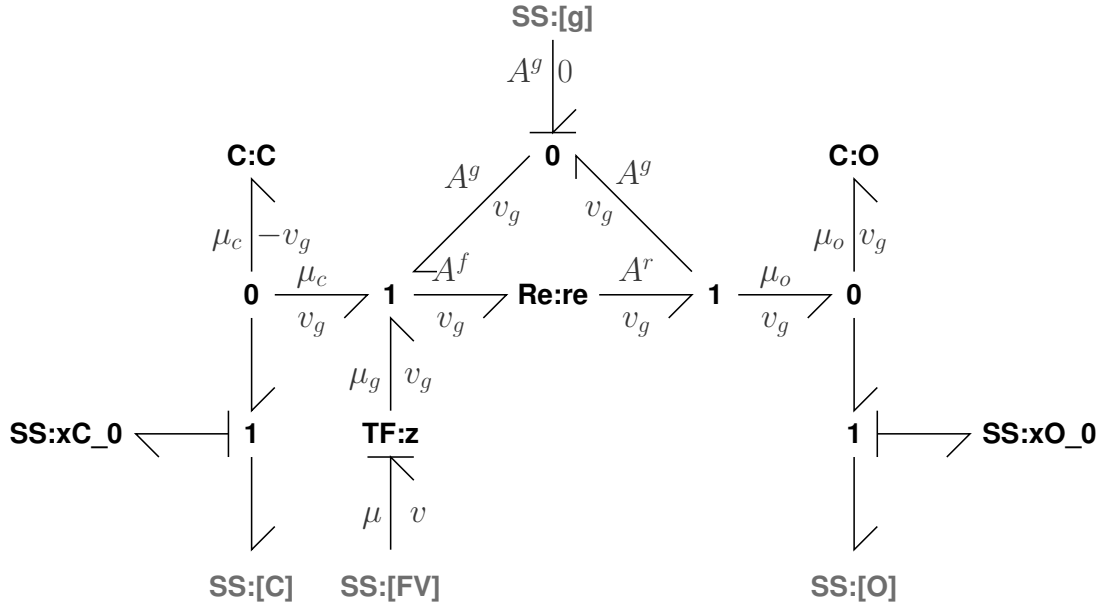
$$\begin{aligned} v_g &= \frac{1}{x_g} \kappa(V) \left(e^{\frac{V}{V_g}} k_c x_c - k_o x_o \right) \\ &= \kappa(V) \left(e^{\frac{V}{V_g}} k_c \left(1 - \frac{x_o}{x_g} \right) - k_o \frac{x_o}{x_g} \right) \end{aligned} \quad (52)$$

The two components **SS**:xC₀ and **SS**:xO₀ both give the constant affinity required to normalise the gate signals between zero and one. The parameters V_g , k_c and k_o , together with the voltage dependent rate constant $\kappa(V)$, can be chosen to fit experimental data. However, unlike the empirical models, Equation (52) is thermodynamically compliant.

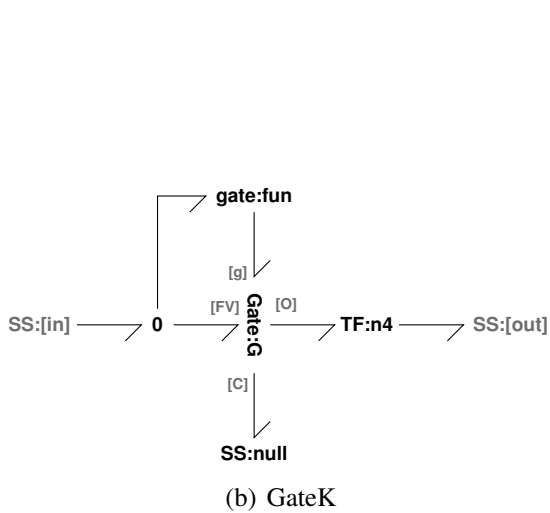
This is illustrated for the three gates (n,m,h) used by Hodgkin and Huxley (19) as listed by Keener and Sneyd (27), Equations 5.24–5.29, where the Bond Graph parameters have been chosen to fit the empirical HH empirical model of the form of Equation (44) or (45). Figures 8(a), 8(c) and 8(e) show g_{ss} for each of the three gates and for both the physical and empirical values. The fit is not exact, as there is no equivalence between the physical gating model and the Hodgkin Huxley empirical model. Figures 8(b), 8(d) and 8(f) show τ for each of the three gates and for both the physical and empirical values; $\kappa(V)$ has been chosen to give an exact fit by making incorporating the empirical expressions for α and β .

Parameter values for these Bond Graph gating models are given in Table 2. Unlike the HH model, the gates themselves draw current from the membrane. The amount of current is partly determined by the total gate states x_g . As the HH model contains no information about gate current, the total gate states x_g are chosen to give a small, but otherwise arbitrary, value.

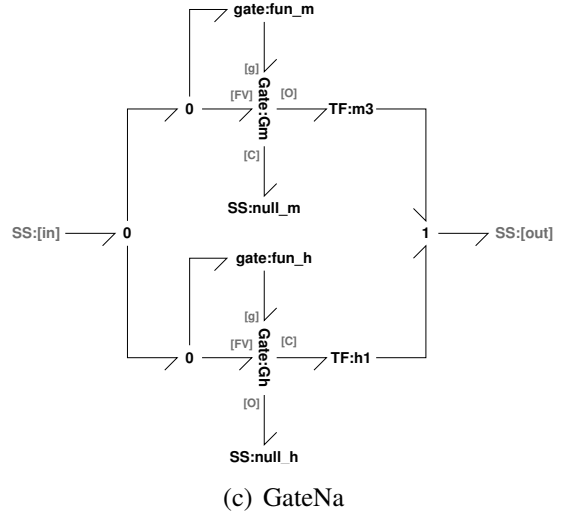
³The pseudo substances may well have a physical interpretation. In particular, x_g seems to be related to ion channel density; see the discussion by Hodgkin (20) and Hille (18, Chap. 12.)



(a) Gate

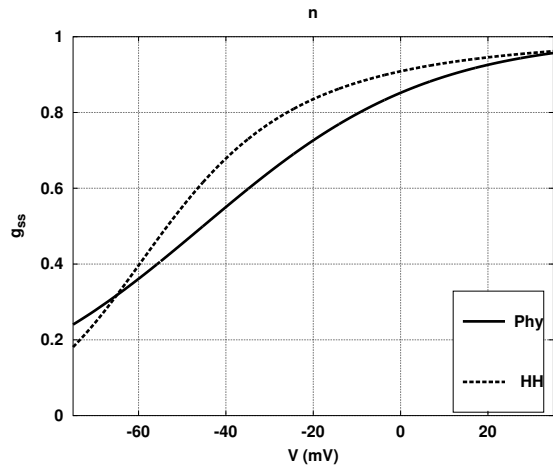


(b) GateK

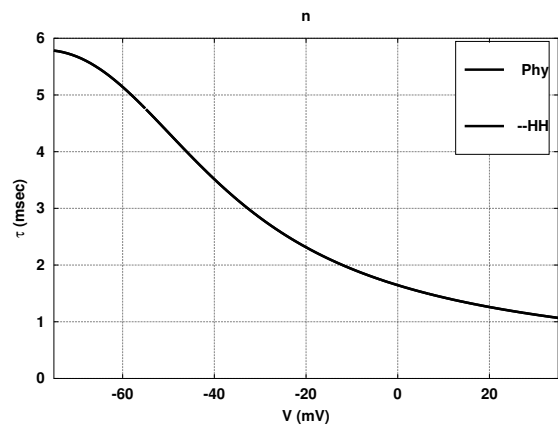


(c) GateNa

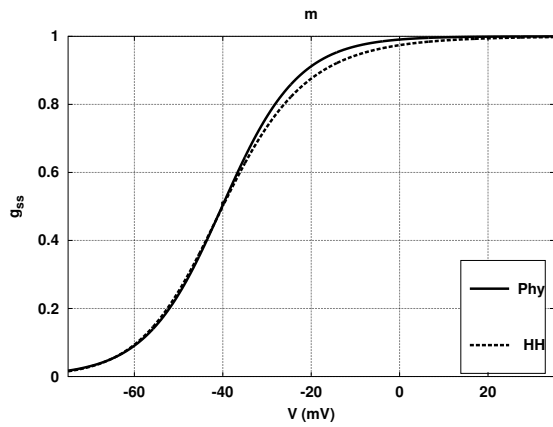
Figure 7: Bond Graph model for physically-plausible gating. (a) The voltage-modulated gate is modelled in a similar way the the ion channel of Figure 4. (b) The basic gate of (a) is used in the K^+ gate. The open state is used and the closed state discarded. The gate equations (44) are implemented in **gate** and the n^4 factor of Equation (48) by **TF:n4**. (c) The basic gate of (a) is used in the Na^+ gate. There are separate models for the m and h gates. The m^3 factor of Equation (49) by **TF:m3**.



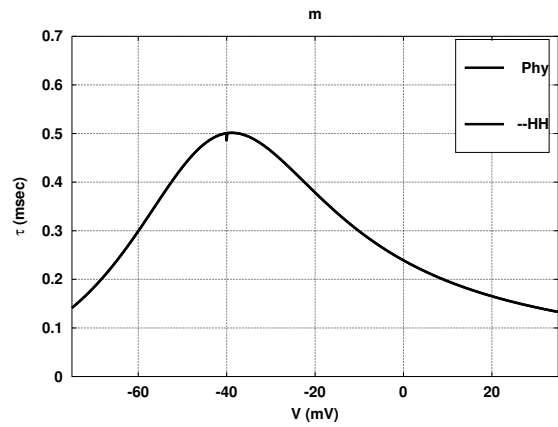
(a) n-gate g_{ss}



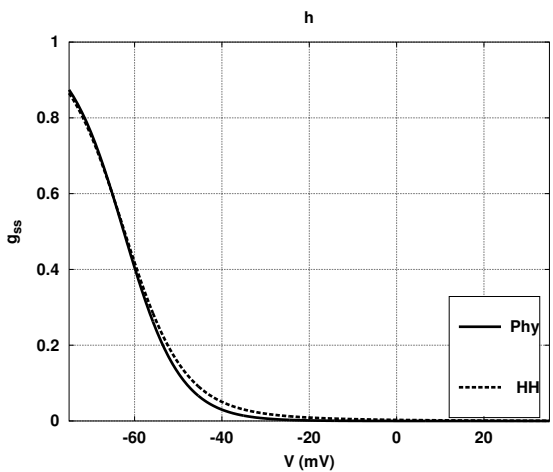
(b) n-gate τ



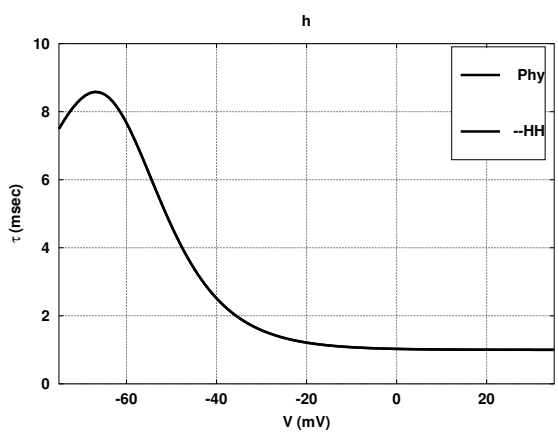
(c) m-gate g_{ss}



(d) m-gate τ



(e) h-gate g_{ss}



(f) h-gate τ

Figure 8: Physical Gate Models fitted to Hodgkin-Huxley equations.

| Parameter | n | m | h |
|-----------|-----------|-----------|-------------------------|
| z_g | 1 | 3 | 4 |
| k_c | 5.7537 | 105.49 | 1 |
| k_o | 1 | 1 | 6.3281×10^{-5} |
| x_g | 10^{-9} | 10^{-9} | 10^{-9} |

Table 2: Physical-model parameters

2.6 Energy Flow in the Hodgkin Huxley Action Potential

We are now in a position to reimplement the Hodgkin and Huxley (19) model as a physically-plausible model using the bond graph formulation. ⁴ Figure 9 shows the bond graph representation of the Hodgkin-Huxley model, consisting of three ion channels (displayed in Figure 6) together with the electrogenic capacitor. These four components share the same electrogenic potential and thus are connected to **0** junctions.

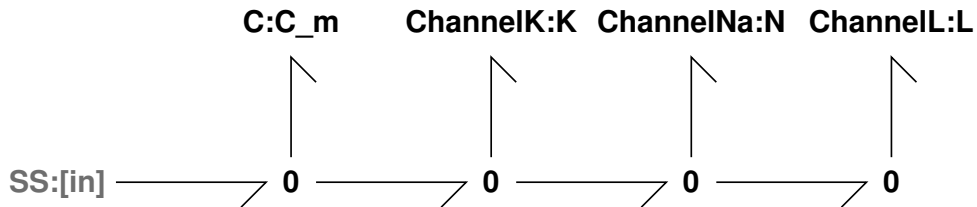


Figure 9: Membrane model

| | K^+ | Na^+ |
|----------|-------|--------|
| Internal | 397 | 50 |
| External | 20 | 437 |

Table 3: Concentrations used in simulation (mM) (27, Table 2.1)

The model has 13 states compared to the 4 states of the HH model. For direct comparison with the HH model, the six states corresponding the internal and external amounts (concentrations) of K^+ , Na^+ and L were fixed at constant values by applying appropriate external flows. Using stoichiometric analysis, the remaining conserved moieties reduce the number of independent states to 4 – the same as the original Hodgkin Huxley model. The reduced order system equation Gawthrop and Crampin (14, (3.48)) was implemented numerically, and was simulated using the parameters given by Keener and Sneyd (27, Chap. 5). The model flows were scaled by a factor of 10^{-9} within the simulation for numerical reasons. The membrane was initially disturbed from the resting potential by a depolarisation of 20mV. The internal and external con-

⁴Following the interpretation of the model of Hodgkin and Huxley (19) given by Keener and Sneyd (27, Chapter 5), an area of 1cm^2 of axon is modelled. The parameters used in this paper are those given by Keener and Sneyd (27, Chapter 5).

concentrations are taken from Keener and Sneyd (27, Table 2.1) and are given in Table 3. Figure 10 shows the response in the electrical domain.

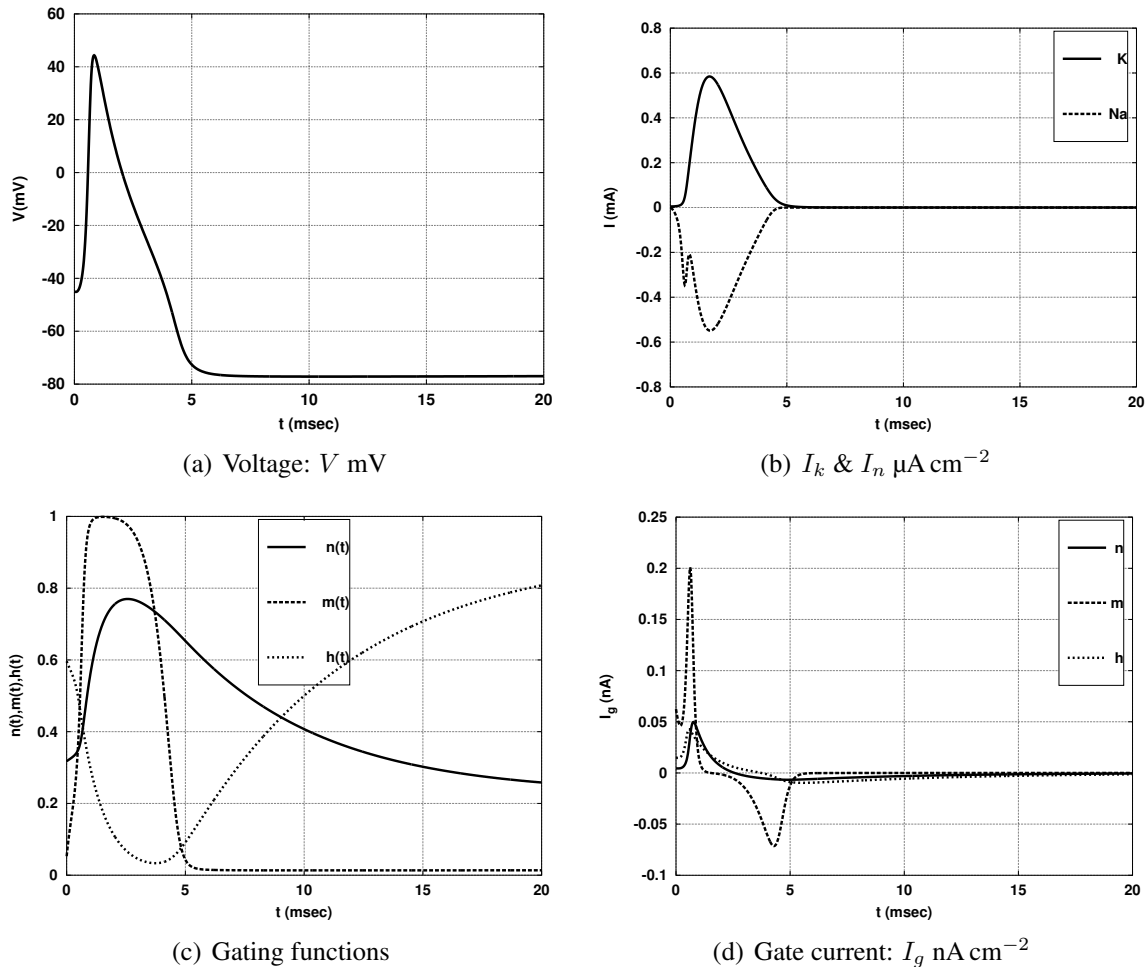


Figure 10: Membrane response: electrical domain. (a) The membrane voltage (mV) is plotted against time (msec) for a single action potential. (b) The corresponding channel currents I_k & I_n ($\mu\text{A cm}^{-2}$). (c) The corresponding three gating functions n , m and h . (d) The gate currents for the three gates (nA cm^{-2}).

In order to calculate the energy flows associated with these ionic movements, Gawthrop et al. (15) give formulae for the energy flows in the bond graph of biochemical networks; the formulae required here appear in Equations (9) – (11).

Using the same simulation data as Figure 10, Figure 11(a) shows the external power ($P_e \mu\text{W cm}^{-2}$) due to the flows of K^+ and Na^+ required to keep the concentrations constant and the net rate of energy dissipation ($P_r \mu\text{W cm}^{-2}$). These two powers are approximately the same; the difference is due to transient energy storage in the electrogenic capacitor. The corresponding energy $E_e(t)$

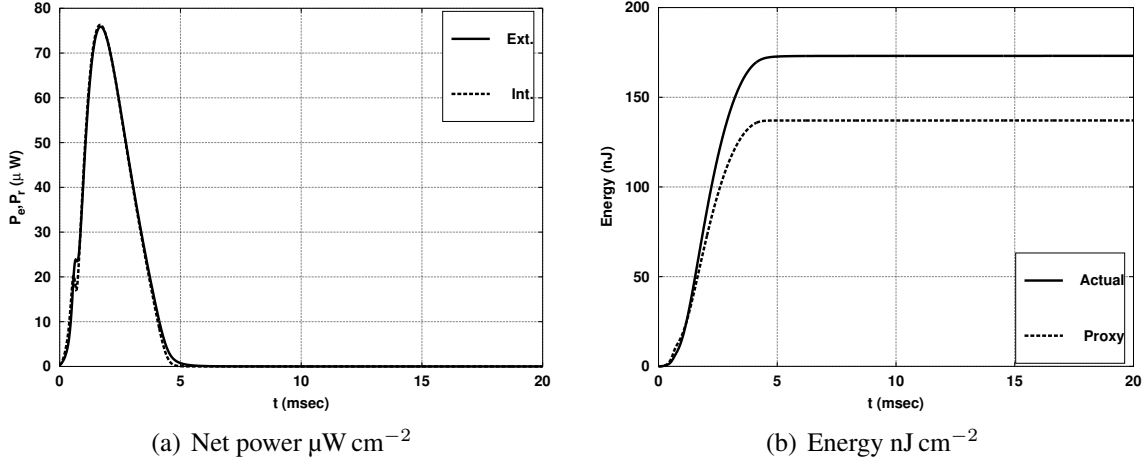


Figure 11: Power & Energy plotted against time (msec). (a) The net external power and dissipated power ($\mu\text{W cm}^{-2}$). (b) The external energy (time integral of external power) and the ATP-proxy energy (nJ cm^{-2}).

of an action potential is computed by integrating the external power P_e with respect to time

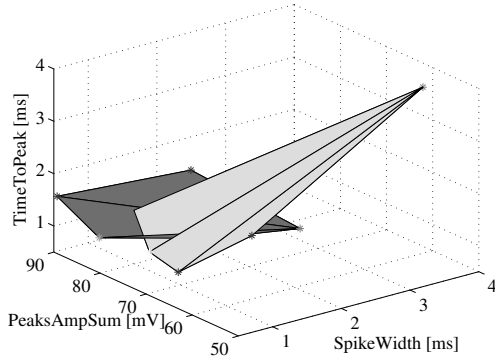
$$E_e(t) = \int_0^t P_e(\tau) d\tau \quad (53)$$

$E_e(t)$ is plotted in Figure 11(b) with the legend “Actual”; the total energy required for this particular model is about 173 nJ cm^{-2} .⁵

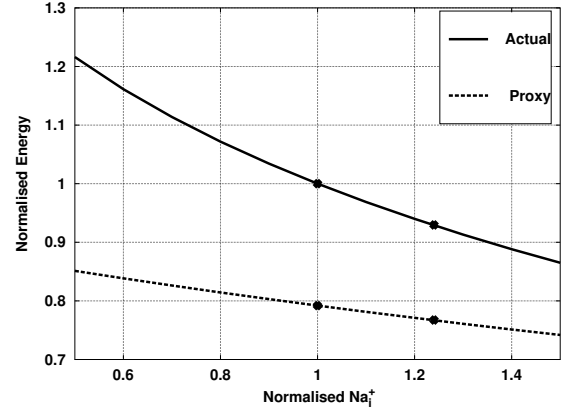
It is interesting to compare this precise method of computing energy dissipation with the ATP proxy approach. The influx of Na^+ (5, 17, 38, 39) is often taken as a proxy for energy consumption. For example, as discussed by Smith and Crampin (43) and Hasenstaub et al. (17), 3Na^+ ions are moved back across the membrane using 1 ATP molecule by the sodium-potassium pump (Na^+ , K^+ , ATPase). Thus the total Na^+ passing through the membrane during an action potential x_n can be taken as a proxy for energy consumption. For example, Hasenstaub et al. (17) use the ATP-proxy x_a via the formula $x_a = \frac{x_n}{3}$. The energy corresponding to the ATP-proxy x_a can be computed from

$$E_a = G_{ATP} x_a \quad (54)$$

where $G_{ATP} \approx 31 \text{ kJ mol}^{-1}$ is the Gibbs free energy associated with the reaction $ATP \rightleftharpoons ADP + Pi$. E_a is plotted in Figure 11(b) together with the actual energy E_e ; the ATP-proxy energy required for this particular model is about 137 nJ cm^{-2} – a discrepancy of about 20% which is discussed in the sequel. Alternatively, this energy requirement could be reexpressed in units of moles of ATP by dividing E_e and E_a by G_{ATP} .



(a) Experimental data



(b) Simulated energy consumption

Figure 12: Retinal Ganglion Cells. (a) Topological manifolds for the parameters of action potentials in WT and RD1 mice. Pale: WT mice; dark: RD1 mice. TimeToPeak is calculated as a difference between the time of the maximum amplitude of an action potential and the time taken for the membrane potential to reach $dV/dt > 10$ mV/ms threshold. PeaksAmpSum is calculated as a sum of the maximum amplitude of an action potential and absolute hyperpolarisation level. (b) Simulated Energy consumption as internal Na^+ concentration varies: the ratio of the energy consumption to the actual energy consumption at the nominal internal Na_i^+ concentration Na_0^+ is plotted against $\text{Na}_i^+/\text{Na}_0^+$ for both actual and proxy energy consumption.

| | Experiments | Simulations |
|------------------|-------------|-------------|
| WT mice | | |
| Vmax [mV] | 23 | 23 |
| Spike Width [ms] | 1.9 | 2 |
| RD1 mice | | |
| Vmax [mV] | 29 | 28 |
| Spike Width [ms] | 1.5 | 1.6 |

Table 4: Comparison of the experimental data and simulation results

2.7 Energy consumption in healthy and degenerative retinal ganglion cells

As discussed in the Supporting Material, *in vitro* data was collected and analysed from retinal ganglion cells (RGCs) of wild-type (WT) and degenerative (RD1) mice. Figure 12(a) illustrates that the experimentally recorded action potentials belong to separate topological manifolds for WT and RD1 mice. This suggests that energy consumption for single action potentials is different for WT and RD1 mice.

Using experimentally fitted parameters as described in the Supporting Material, simulations of both cell types were conducted and a comparison of the experimental data and simulation results is given in Table 4.

The simulation results indicated that \bar{g}_{Na} is increased by at least 24% in degenerative retina. Figure 12(b) shows how actual and ATP-proxy energy varies with internal sodium concentration. The solid line illustrates actual energy consumption, the dashed line illustrates the ATP-proxy calculation, and the crosses indicate data points calculated for RD1 and WT mice energy consumption. Figure 12(b) illustrates that the difference in the normalized energy consumption for one action potential between WT and RD1 RGCs is 0.03 using ATP-proxy methodology, while the difference is 0.08 using methodology proposed in this paper. The figure shows that the ATP-proxy methodology underestimates the energy consumption for both mouse types. In addition, the ATP-proxy methodology underestimates the difference between the two types of mice, while the proposed methodology provides accurate comparison of energy consumption between two similar-shaped action potentials (note the relatively small differences between WT and RD1 cells in Table 4).

3 DISCUSSION

| | K ⁺ | Na ⁺ | K ⁺ + Na ⁺ | ATP |
|---------------------------|----------------|-----------------|----------------------------------|--------|
| x (pmol) | 13.60 | 13.27 | – | 4.42 |
| G (kJ mol ⁻¹) | 7.54 | 3.68 | – | 31 |
| E (nJ) | 101.35 | 71.73 | 173.08 | 137.08 |

Table 5: Simulation results (per cm²). x is the quantity, G the molar free energy and E the energy consumed by the action potential. x_a is computed from the formula $x_a = \frac{x_n}{3}$

We have constructed a Bond Graph model of the Hodgkin and Huxley (19) model of the axon; and we have used this model to show that calculation of energy consumption during generation of the action potential by counting Na⁺ ions crossing the membrane underestimates true energy consumption by around 20%.

In this particular simulation, the concentrations are constant and thus Equation (10) is appropriate. Moreover, the contribution of the leakage and the gating currents are small and can be

⁵ The energy corresponding to the initial depolarisation of $V_0 = 20\text{mV}$ is $\frac{1}{2}C_m V_0^2 = 0.2\text{nJ cm}^{-2}$; this can be neglected in the overall energy balance.

neglected. The values of Table 3 and Equation (10) gives the molar free energy values of Table 5 for K^+ , Na^+ ; that for ATP is taken from Keener and Sneyd (27, (1.23)). Because the actual energy consumption depends on both the amounts of K^+ , Na^+ as well as on the internal and external concentrations, there is no way that the ATP-proxy formula (based on only the amount of Na^+) can give the correct value under all circumstances. To illustrate this, Figure 12 shows how actual and ATP-proxy energy varies with internal Na^+ concentration expressed as a ratio ρ to the nominal concentration of Table 3. The discrepancy between actual and ATP-proxy energy varies with ρ . Moreover, the method of this paper does *not* require the concentrations to be constant during an action potential and is thus applicable to more general situations.

In order to construct the Bond Graph model we have extended our earlier work on Bond Graph modelling of biochemical systems to encompass electrochemical systems. In order to bridge the chemical and electrical domains, we have introduced the electrogenic capacitor, which is an electrical capacitor viewed from the chemical domain.

Although the model is built to approximate that of Hodgkin and Huxley (19), it differs in a number of ways. Firstly the GHK ion channel formulation was used in order to produce a physically plausible model for open channel ion flow. This is a nonlinear approximation to the linear Hodgkin Huxley ion channel model. Secondly, gating currents are explicitly included, again in order to produce a thermodynamically consistent model. Finally, the Bond Graph model must also allow for *varying* concentrations of Na^+ and K^+ .

The significance of our approach is to that it provides a framework within which biophysically based models are robustly thermodynamically compliant (15), as required for example when considering the energetic costs and consequences of cellular biological processes. Furthermore, the Bond Graph approach provides a basis for modular modelling of large, multi-domain electro-chemical biological systems, such as is now commonplace in systems biology models of excitable membranes in the neuronal and cardiac context. Components and modules which are represented as Bond Graphs are physically plausible models which obey the basic principles of thermodynamics, and therefore larger models constructed from such modules will also consequentially be physically plausible models. Future work will further develop these concepts in order to represent ligand-gated ion channels, ion pumps (such as the Ca^{2+} pump SERCA (14, 47) and the Na^+ pump (43, 46), as are required for current generation neuronal and cardiac cell models. This modular approach allows simpler modules to be replaced by more complex modules, or empirical modules to be replaced by physically-based modules, as the underlying science advances.

Furthermore, the multi-domain nature of Bond Graphs makes possible extension of the approach to mechano-chemical transduction. In actively contracting cardiac muscle, for example, energetic considerations are dominated by force production, where approximately 75–80% of ATP consumption in cardiomyocytes over a cardiac cycle is due to formation of contractile cross-bridges, 5–10% due to the Na^+ pump, and Ca^{2+} extrusion and uptake into Ca^{2+} stores accounting for the remainder (48). In cardiac muscle, energetics is known to play a critical role in the health of cardiac muscle, with many studies implicating energetic imbalance or inadequacy of energy production in heart disease (33). Models which provide a mechanism with which to assess the energetic aspects of cell function are therefore much needed. Combining metabolism, electro-chemical and chemo-mechanical energy transduction to examine energy flows within the

heart (26, 33) is therefore a major goal of our work.

The ATP-proxy approach is based on assuming that the biological entity is operating in a normal state and therefore could lead to misleading conclusions in a pathophysiological state. In contrast, our approach makes no assumption of normality and may be expected to be of use in pathophysiological states in general and, in particular, the retinal example discussed in this paper. Our use of the RD1 degenerate retina mouse model ensures that the outcomes of this project are directly relevant to human patients since RD1 mice have a degenerate retina that has distinct similarities to that observed in human patients with *retinitis pigmentosa* – a set of hereditary retinal diseases that results from the degenerative loss of the photoreceptors in the retina. It has been proposed that the death of rod photoreceptors results in decreased oxygen consumption (42). In addition, it has been shown that potassium channel-opening agents directly affect mitochondria (29). Therefore, it is important to understand how energy consumption in degenerative retina is altered. The proposed methodology allows a comparison between the energy consumption in healthy and degenerate mice, even when the differences in action potentials between the two types are small.

Finally, we have shown in this study that building Bond Graph models in this way provides a mechanism for direct evaluation of energy dissipation as estimated from the model. We suggest that using the actual, rather than the proxy, energy dissipation would seem to be a more accurate, and generally more reliable, approach. It would therefore be interesting to reexamine the optimality arguments of Hasenstaub et al. (17) and Sengupta and Stemmler (38) using this approach.

4 ACKNOWLEDGEMENTS

Peter Gawthrop would like to thank the Melbourne School of Engineering for its support via a Professorial Fellowship. This research was in part conducted and funded by the Australian Research Council Centre of Excellence in Convergent Bio-Nano Science and Technology (project number CE140100036), and by the Virtual Physiological Rat Centre for the Study of Physiology and Genomics, funded through NIH grant P50-GM094503.

5 AUTHOR CONTRIBUTIONS

The theory was developed by PJG, IS and EC. The theoretical part of the paper was written by PJG, IS and EC and the experimental part by TK. Experiments were conducted by SS and MI.

6 DATA ACCESSIBILITY

A virtual reference environment (22) is available for this paper at https://github.com/uomsystemsbiology/energetic_cost_reference_environment.

References

1. Peter Atkins and Julio de Paula. *Physical Chemistry for the Life Sciences*. Oxford University Press, 2nd edition, 2011.
2. David Attwell and Simon B. Laughlin. An energy budget for signaling in the grey matter of the brain. *J Cereb Blood Flow Metab*, 21:1133–1145, October 2001. ISSN 0271-678X. doi: 10.1097/00004647-200110000-00001.
3. M. Flint Beal. Does impairment of energy metabolism result in excitotoxic neuronal death in neurodegenerative illnesses? *Annals of Neurology*, 31(2):119–130, 1992. ISSN 1531-8249. doi: 10.1002/ana.410310202.
4. Wolfgang Borutzky. *Bond Graph Modelling of Engineering Systems: Theory, Applications and Software Support*. Springer, 2011. ISBN 9781441993670.
5. Brett C. Carter and Bruce P. Bean. Sodium entry during action potentials of mammalian neurons: Incomplete inactivation and reduced metabolic efficiency in fast-spiking neurons. *Neuron*, 64(6):898 – 909, 2009. ISSN 0896-6273. doi: 10.1016/j.neuron.2009.12.011.
6. William A Catterall, Indira M Raman, Hugh PC Robinson, Terrence J Sejnowski, and Ole Paulsen. The Hodgkin-Huxley heritage: from channels to circuits. *The Journal of Neuroscience*, 32(41):14064–14073, 2012. doi: 10.1523/JNEUROSCI.3403-12.2012.
7. F. E. Cellier. *Continuous system modelling*. Springer-Verlag, 1991.
8. F. E. Cellier. Hierarchical non-linear bond graphs: a unified methodology for modeling complex physical systems. *SIMULATION*, 58(4):230–248, 1992. doi: 10.1177/003754979205800404.
9. M. Cloutier, R. Middleton, and P. Wellstead. Feedback motif for the pathogenesis of Parkinson’s disease. *Systems Biology, IET*, 6(3):86–93, June 2012. ISSN 1751-8849. doi: 10.1049/iet-syb.2011.0076.
10. Mathieu Cloutier, B. Bolger, Fiachra, P. Lowry, John, and Peter Wellstead. An integrative dynamic model of brain energy metabolism using in vivo neurochemical measurements. *Journal of Computational Neuroscience*, 27(3):391–414, 2009. ISSN 0929-5313. doi: 10.1007/s10827-009-0152-8.
11. P. J. Gawthrop and L. P. S. Smith. *Metamodelling: Bond Graphs and Dynamic Systems*. Prentice Hall, Hemel Hempstead, Herts, England., 1996. ISBN 0-13-489824-9.
12. Peter J Gawthrop. Physically-plausible models for identification. In *Proceedings of the 2003 International Conference On Bond Graph Modeling and Simulation (ICBGM’03)*, Simulation Series, Orlando, Florida, U.S.A., January 2003. Society for Computer Simulation.

13. Peter J Gawthrop and Geraint P Bevan. Bond-graph modeling: A tutorial introduction for control engineers. *IEEE Control Systems Magazine*, 27(2):24–45, April 2007. doi: 10.1109/MCS.2007.338279.
14. Peter J. Gawthrop and Edmund J. Crampin. Energy-based analysis of biochemical cycles using bond graphs. *Proceedings of the Royal Society A: Mathematical, Physical and Engineering Science*, 470(2171), 2014. doi: 10.1098/rspa.2014.0459.
15. Peter J. Gawthrop, Joseph Cursons, and Edmund J. Crampin. Hierarchical bond graph modelling of biochemical networks. *Proceedings of the Royal Society of London A: Mathematical, Physical and Engineering Sciences*, 471(2184), 2015. ISSN 1364-5021. doi: 10.1098/rspa.2015.0642. Available at arXiv:1503.01814.
16. J. Greifeneder and F.E. Cellier. Modeling chemical reactions using bond graphs. In *Proceedings ICBGM12, 10th SCS Intl. Conf. on Bond Graph Modeling and Simulation*, pages 110–121, Genoa, Italy, 2012.
17. Andrea Hasenstaub, Stephani Otte, Edward Callaway, and Terrence J. Sejnowski. Metabolic cost as a unifying principle governing neuronal biophysics. *Proceedings of the National Academy of Sciences*, 107(27):12329–12334, 2010. doi: 10.1073/pnas.0914886107.
18. Bertil Hille. *Ion Channels of Excitable Membranes*. Sinauer Associates, Sunderland, MA, USA, 3rd edition, 2001. ISBN 978-0-87893-321-1.
19. A. L. Hodgkin and A. F. Huxley. A quantitative description of membrane current and its application to conduction and excitation in nerve. *The Journal of Physiology*, 117(4):500–544, 1952.
20. Alan Hodgkin. The optimum density of sodium channels in an unmyelinated nerve. *Philosophical Transactions of the Royal Society B: Biological Sciences*, 270(908):297–300, 1975.
21. Clare Howarth, Pdraig Gleeson, and David Attwell. Updated energy budgets for neural computation in the neocortex and cerebellum. *J Cereb Blood Flow Metab*, 32:1222–1232, July 2012. ISSN 0271-678X. doi: 10.1038/jcbfm.2012.35.
22. Daniel G. Hurley, David M. Budden, and Edmund J. Crampin. Virtual reference environments: a simple way to make research reproducible. *Briefings in Bioinformatics*, 2014. doi: 10.1093/bib/bbu043.
23. Tatiana Kameneva, Hamish Meffin, and AnthonyN. Burkitt. Modelling intrinsic electrophysiological properties of on and off retinal ganglion cells. *Journal of Computational Neuroscience*, 31(3):547–561, 2011. ISSN 0929-5313. doi: 10.1007/s10827-011-0322-3.
24. Dean Karnopp. Bond graph models for electrochemical energy storage : electrical, chemical and thermal effects. *Journal of the Franklin Institute*, 327(6):983 – 992, 1990. ISSN 0016-0032. doi: 10.1016/0016-0032(90)90073-R.

25. Dean C Karnopp, Donald L Margolis, and Ronald C Rosenberg. *System Dynamics: Modeling, Simulation, and Control of Mechatronic Systems*. John Wiley & Sons, 5th edition, 2012. ISBN 978-0470889084.
26. Arnold M Katz. *Physiology of the Heart*. Lippincott Williams and Wilkins, Philadelphia, fifth edition, 2011. ISBN 978-1-60831-171-2.
27. James P Keener and James Sneyd. *Mathematical Physiology: I: Cellular Physiology*, volume 1. Springer, 2nd edition, 2009.
28. Christof Koch. *Biophysics of computation: information processing in single neurons*. Oxford University Press, Oxford, 2004.
29. Bogusz Kulawiak, Alexei P. Kudin, Adam Szewczyk, and Wolfram S. Kunz. BK channel openers inhibit ROS production of isolated rat brain mitochondria. *Experimental Neurology*, 212(2):543 – 547, 2008. ISSN 0014-4886. doi: <http://dx.doi.org/10.1016/j.expneurol.2008.05.004>.
30. A. G. J. MacFarlane. *Engineering Systems Analysis*. G. G. Harrap, Cambridge, Mass., 1964.
31. J.C. Maxwell. Remarks on the mathematical classification of physical quantities. *Proceedings London Mathematical Society*, pages 224–233, 1871.
32. Amalendu Mukherjee, Ranjit Karmaker, and Arun Kumar Samantaray. *Bond Graph in Modeling, Simulation and Fault Identification*. I.K. International, New Delhi,, 2006.
33. Stefan Neubauer. The failing heart – an engine out of fuel. *New England Journal of Medicine*, 356(11):1140–1151, 2007. doi: 10.1056/NEJMra063052.
34. Jeremy E. Niven and Simon B. Laughlin. Energy limitation as a selective pressure on the evolution of sensory systems. *Journal of Experimental Biology*, 211(11):1792–1804, 2008. ISSN 0022-0949. doi: 10.1242/jeb.017574.
35. George Oster, Alan Perelson, and Aharon Katchalsky. Network thermodynamics. *Nature*, 234:393–399, December 1971. doi: 10.1038/234393a0.
36. George F. Oster, Alan S. Perelson, and Aharon Katchalsky. Network thermodynamics: dynamic modelling of biophysical systems. *Quarterly Reviews of Biophysics*, 6(01):1–134, 1973. doi: 10.1017/S0033583500000081.
37. Steven J Schiff. *Neural control engineering*. MIT press, Cambridge, 2011. ISBN 9780262312080.
38. B. Sengupta and M.B. Stemmler. Power consumption during neuronal computation. *Proceedings of the IEEE*, 102(5):738–750, May 2014. ISSN 0018-9219. doi: 10.1109/JPROC.2014.2307755.

39. Biswa Sengupta, Martin Stemmler, Simon B. Laughlin, and Jeremy E. Niven. Action potential energy efficiency varies among neuron types in vertebrates and invertebrates. *PLoS Comput Biol*, 6(7):e1000840, 07 2010. doi: 10.1371/journal.pcbi.1000840.
40. Biswa Sengupta, Martin B. Stemmler, and Karl J. Friston. Information and efficiency in the nervous system synthesis. *PLoS Comput Biol*, 9(7):e1003157, 07 2013. doi: 10.1371/journal.pcbi.1003157.
41. J. L. Shearer, A. T. Murphy, and H. H. Richardson. *Introduction to System Dynamics*. Addison-Wesley, Reading, Massachusetts, 1971.
42. JiKui Shen, Xiaoru Yang, Aling Dong, Robert M. Petters, You-Wei Peng, Fulton Wong, and Peter A. Campochiaro. Oxidative damage is a potential cause of cone cell death in retinitis pigmentosa. *Journal of Cellular Physiology*, 203(3):457–464, 2005. ISSN 1097-4652. doi: 10.1002/jcp.20346.
43. N.P. Smith and E.J. Crampin. Development of models of active ion transport for whole-cell modelling: cardiac sodium-potassium pump as a case study. *Progress in Biophysics and Molecular Biology*, 85(2-3):387 – 405, 2004. doi: 10.1016/j.pbiomolbio.2004.01.010.
44. David Sterratt, Bruce Graham, Andrew Gillies, and David Willshaw. *Principles of Computational Modelling in Neuroscience*. Cambridge University Press, 2011. ISBN 9780521877954.
45. K. H. W. J. ten Tusscher, D. Noble, P. J. Noble, and A. V. Panfilov. A model for human ventricular tissue. *American Journal of Physiology - Heart and Circulatory Physiology*, 286(4):H1573–H1589, 2004. ISSN 0363-6135. doi: 10.1152/ajpheart.00794.2003.
46. Jonna R. Terkildsen, Steven Niederer, Edmund J. Crampin, Peter Hunter, and Nicolas P. Smith. Using physiome standards to couple cellular functions for rat cardiac excitation-contraction. *Experimental Physiology*, 93(7):919–929, 2008. ISSN 1469-445X. doi: 10.1113/expphysiol.2007.041871.
47. Kenneth Tran, Nicolas P. Smith, Denis S. Loiselle, and Edmund J. Crampin. A thermodynamic model of the cardiac sarcoplasmic/endoplasmic Ca²⁺ (SERCA) pump. *Biophysical Journal*, 96(5):2029 – 2042, 2009. ISSN 0006-3495. doi: 10.1016/j.bpj.2008.11.045.
48. Kenneth Tran, Denis S. Loiselle, and Edmund J. Crampin. Regulation of cardiac cellular bioenergetics: mechanisms and consequences. *Physiological Reports*, 3(7):e12464, 2015. ISSN 2051-817X. doi: 10.14814/phy2.12464.
49. Pierre Van Rysselberghe. Reaction rates and affinities. *The Journal of Chemical Physics*, 29(3):640–642, 1958. doi: 10.1063/1.1744552.
50. Henning U. Voss, Jens Timmer, and Jrgen Kurths. Nonlinear dynamical system identification from uncertain and indirect measurements. *International Journal of Bifurcation and Chaos in Applied Sciences and Engineering*, 14(6):1905 – 1933, 2004. ISSN 02181274.

51. P. E. Wellstead. *Introduction to Physical System Modelling*. Academic Press, 1979.
52. Peter Wellstead. *A New Look at Disease: Parkinson's through the eyes of an engineer*. Control Systems Principles, Stockport, UK, 2012. ISBN 978-0-9573864-0-2.
53. Peter Wellstead and Mathieu Cloutier, editors. *Systems Biology of Parkinson's Disease*. Springer New York, 2012. ISBN 978-1-4614-3411-5. doi: 10.1007/978-1-4614-3411-5.

A SUPPORTING MATERIAL

A.1 Example: Application of the proposed methodology to calculate the energy consumption in healthy and degenerative retinal ganglion cells

A.1.1 Methods

Experiments

In vitro data was collected and analysed from retinal ganglion cells (RGCs) of wild-type (WT) (n=8) and degenerative RD1 (n=6) mice 4 - 4.5 month old. Experimental procedures were approved by the animal welfare committee at the University of Melbourne and are in accordance with local and national guidelines for animal care. Animals were housed in temperature-regulated facilities on a 12h light/dark cycle in the animal house and had plentiful access to food and water. Neither WT nor RD1 mice were dark adapted for these experiments.

Retinae from WT and RD1 mice were treated identically. Mice were anaesthetized with simultaneous ketamine (67 mg/kg) and xylazine (13 mg/kg) injections, the eyes were enucleated and then the mice were killed by cervical dislocation. Their eyes were bathed in carbogenated (95% O₂ and 5% CO₂) Ames' medium (Sigma-Aldrich, St. Louis, MO), hemisected at the ora serata, and the cornea and lens were removed. The retina was continuously superfused with carbogenated Ames medium at a rate of 4-8 ml/min. All of the procedures were performed at room temperature and in normal room light.

The flat-mount retina was viewed through the microscope with the use of Nomarski DIC optics and also on a video monitor with additional 4x magnification using a CCD camera (Ikegami, ICD-48E). For whole cell recording, a small opening was first made with a sharp tip pipette (resistance above 14 M Ω) through the inner limiting membrane and optic fibre layer that covered a selected retinal ganglion cell. Prior to recording, the pipette voltage in the bath was nullified. The pipette series resistance was measured and compensated for using standard amplifier circuitry (SEC-05x; NPI Electronic Instruments). Pipette resistance was in the range of 7-14 M Ω for all experiments. Membrane potentials were amplified (as above with SEC-05x, npi) and digitized at 50 kHz (USB-6221, National Instruments), acquired and stored in digital form by custom software developed in Matlab (Mathworks).

Modelling

To calculate the energy consumption in WT and RD1 RGCs, Hodgkin-Huxley-type model parameters were fitted to the experimental data described above. Experimentally recorded maximum amplitude and width of spontaneous action potentials in two groups were averaged and used for model constraints.

A variety of voltage-gated ionic currents in RGCs have been identified experimentally: a calcium current (I_{Ca}), three types of potassium currents (A-type (I_{K_A}), Ca-activated ($I_{K(Ca)}$), and delayed rectifier (I_K)), T-type Ca²⁺ (I_T), hyperpolarization-activated (I_h) and leakage (I_L) currents. The equation governing the membrane potential, V , was obtained by summing all membrane currents using Kirchoff's law,

$$C_m \frac{dV}{dt} + I_{Na} + I_{Ca} + I_{K,A} + I_{K(Ca)} + I_K$$

$$+ I_T + I_h + I_L = 0, \quad (55)$$

where C_m a specific membrane capacitance. The dynamics of each voltage-gated ionic current are governed by Hodgkin-Huxley-type gating variables, which are described by first-order kinetic equations as given in (23), but are omitted here for brevity.

In this study, we sought to account for the differences in the energy consumption between WT and RD1 RGCs on the basis of differences in the magnitudes of the maximal conductance of sodium and potassium currents, \bar{g}_{Na} and \bar{g}_K respectively. While all other parameters were kept fixed, \bar{g}_{Na} and \bar{g}_K were systematically varied in the range $[10^{-15}, 0.1]$ in variable steps (higher resolution for smaller values). For conservative calculation of the difference in the energy consumption, the smallest difference between \bar{g}_{Na} and \bar{g}_K in WT and RD1 types that replicated experimental data is reported here. Model parameters used in simulations are given in Table 5; \bar{g}_i , V_i are maximum conductance and reversal potential of the current “i”. V_{Ca} and $\bar{g}_{K(Ca)}$ depend on the intracellular Ca^{2+} concentration. A single-compartment Hodgkin-Huxley type neurons was simulated in NEURON. The standard Euler integration method was used in simulations. Data was analyzed in Matlab (Mathworks).

Table 5. Simulation parameters.

| | |
|-------------------------------------|--|
| $T = 22^{\circ} C$ | $C_m = 1 \mu F/cm^2$ |
| $V_{Na} = 35 \text{ mV}$ | \bar{g}_{Na} is varied in simulations |
| V_{Ca} is variable, refer to (23) | $\bar{g}_{Ca} = 2.2 \cdot 10^{-3} \text{ S/cm}^2$ |
| $V_K = -70 \text{ mV}$ | \bar{g}_K is varied in simulations |
| | $\bar{g}_{K,A} = 3.6 \cdot 10^{-2} \text{ S/cm}^2$ |
| | $\bar{g}_{K(Ca)}$ is variable, refer to (23) |
| $V_L = -60 \text{ mV}$ | $\bar{g}_L = 10^{-6} \text{ S/cm}^2$ |
| $V_h = 0 \text{ mV}$ | $\bar{g}_h = 10^{-7} \text{ S/cm}^2$ |
| $V_T = 120 \text{ mV}$ | $\bar{g}_T = 10^{-3} \text{ S/cm}^2$ |

The following simulation pa-

rameters reproduced the maximum amplitude and width of the experimentally recorded action potentials in WT and RD1 mice and gave the smallest difference in values between the two retina types. Parameters for WT: $\bar{g}_{Na} = 0.0342 \text{ S/cm}^2$, $\bar{g}_K = 0.0102 \text{ S/cm}^2$. Parameters for RD1: $\bar{g}_{Na} = 0.0422 \text{ S/cm}^2$, $\bar{g}_K = 0.0102 \text{ S/cm}^2$.